ACCURATE PREDICTION OF YIELD STRENGTH AND WELDING DEFECTS IN FSW JOINTS OF 2XXX AND 6XXX AL ALLOYS USING ARTIFICIAL NEURAL NETWORK BASED CORRELATION ANALYSIS

A. K. Deepati[1], P. Anusha[2], M. Naga Swapna Sri[2], S. Guharaja[3], S. Vijayakumar[4,*]

[1]Department of Mechanical Engineering Technology, CAIT, Jazan University, Jizan, Kingdom of Saudi Arabia
[2]Department of Mechanical Engineering, Prasad V. Potluri Siddhartha Institute of Technology, Vijayawada, India
[3]Department of Mechanical Engineering, R.V.S. College of Engineering, Dindigul, India
[4]Mechanical Engineering Department, Saveetha School of Engineering, SIMATS, Tamil Nadu, India
*Corresponding author's e-mail address: vijaysundarbe@gmail.com

ABSTRACT

The accurate prediction of mechanical properties and defect formation in friction stir welding (FSW) of aluminium alloys is crucial for ensuring structural integrity and reliability in aerospace and automotive applications. In this study, an artificial neural network (ANN) was developed to predict yield strength (YS) and welding defects (WD) in FSW joints of AA2024, AA2219, and AA6061 alloys. A dataset of one hundred experimental cases obtained from peer-reviewed literature was employed, where process parameters rotational speed (RS), plate thickness (PT), shoulder radius (SR), axial pressure (AP), pin root radius (PR), pin tip radius (PS), and tool angle (TA) were served as inputs, and YS and WD were target outputs. The ANN was implemented in MATLAB R2016a and trained using backpropagation. Results showed strong predictive accuracy: for YS, correlation coefficients (R) of 0.96568, 0.99874, and 0.96278 were achieved for training, validation, and testing sets, with an overall R of 0.96764. The minimum validation error (MSE = 2.1901) occurred at epoch 11. For WD prediction, the overall R was 0.83229, with lowest validation error (MSE = 0.09041) at epoch 17. These findings highlight the potential of ANN-based models for real-time prediction and optimization of FSW quality. Future work will focus on expanding datasets, integrating hybrid AI techniques, and developing adaptive models for industrial-scale welding applications.

KEYWORDS: friction stir welding**,** aluminium alloys, MATLAB, artificial neural network, correlation coefficients and minimum validation error.

1. INTRODUCTION

Welding processes are critical in modern industries because they help to minimize complexity and reduce the size of mechanical components. However, conventional fusion welding of aluminium alloys is often challenged by problems such as hot cracking, porosity, and embrittlement along the joints due to the high thermal and electrical conductivity of aluminium [1-2]. To overcome these limitations, Friction Stir Welding (FSW) has emerged as an effective alternative, offering superior joint quality with minimal distortion and improved sustainability. The rotating tool in FSW with forward motion generates intense frictional heat and plastic deformation, raising the temperature to around 420-480 °C - sufficient to soften the material without reaching its melting point [3-6].

Generally, the aluminium metal is one of the most important lightweight engineering materials and it has low density and excellent recyclability. It is used in high-performance sectors such as defence, transportation, aviation and aerospace. Despite these advantages, its relatively lower strength compared to steel limits its direct structural applications, thereby imposing the development of alloying systems to improve its mechanical performance. Depending on the composition and processing route, aluminium alloys can be broadly classified into heat-treatable and non-heat-treatable systems, each offering distinct advantages for specific applications. These alloys are widely used in structures requiring a balance of lightweight properties, strength, and formability, make them essential materials for advanced manufacturing and engineering [7].

Date of submission/acceptance: 18.08.2025/15.12.2025
https://doi.org/10.35219/awet.2025.09

The selection of parameters in FSW process is critical to determine the quality, strength, and appearance of the weld, as well as the overall process efficiency [8-9]. For instance, an optimal tool rotation speed ensures sufficient frictional heat for proper material softening, while an appropriate traverse speed balances heat input and also influences nugget size, the thermo-mechanically affected zone (TMAZ) width, and precipitates distribution, while welding speed strongly affects defect formation and tensile efficiency [10-11]. The tool pin profile and shoulder dimensions critically modify stirring intensity and heat generation, with square and triflate pins enhancing material mixing and defect-free consolidation, particularly in dissimilar aluminium combinations such as AA6061–AA5086 [12] and larger shoulders improved consolidation but risking overheating [13].

The axial force, plunge depth, and tilt angle directly influence contact pressure, heat input, and forging action, thereby affecting void elimination and dynamic recrystallization kinetics [14]. Excessive heat input can lead to precipitate coarsening in precipitation-hardened alloys, reducing tensile strength, whereas insufficient heat promotes tunnel defects and lack of bonding [15]. Incorrect parameter combinations can lead to defects such as voids, tunnel defects, or excessive flash, whereas optimized settings promote fine, equiaxed grains in the weld nugget, enhancing strength and ductility [16-17]. Accurate prediction of mechanical properties and defects in friction stir welding (FSW) has been achieved using a range of techniques. For example, Statistical design approaches such as Response Surface Methodology (RSM) and Taguchi–Grey Relational Analysis (GRA) have been widely applied to develop empirical models for outputs like ultimate tensile strength (UTS), hardness, and elongation, providing clear parameter-effect relationships and multi-response optimization capabilities [15], [18]. Proper optimization can refine the weld nugget's grain structure, improve tensile strength and ductility, while also reducing the tool wear and enhancing the productivity. Moreover, parameter selection must consider material type, thickness, and joint configuration, as each affects heat flow and stirring efficiency. Therefore, careful parameter optimization is essential to achieve high-quality, reliable, and reproducible FSW joints across diverse materials and applications [19]. Classical machine-learning algorithms, including Support Vector Machines (SVM), Random Forests (RF), and ensemble models have shown strong predictive accuracy for UTS and hardness in both symmetric and asymmetric welds, with ensemble methods often outperforming single learners while maintaining robustness against overfitting [20]. Artificial neural networks (ANNs) have been extensively applied in welding process prediction due to their capability to model nonlinear relationships between process parameters, material properties, and weld quality. Feed-forward ANNs trained with inputs such as tool geometry, rotation speed, and travel speed have successfully predicted mechanical properties and also compared ANNs to ANFIS and reporting ANNs' competitive or superior accuracy [21-23]. A. Scotti. et al. [24] utilized arc-voltage time series as input data for ANN models to achieve real-time weld quality monitoring and defect detection, which provided a foundation for automated and intelligent welding systems and they have been employed to predict weld strength and deformation, and when coupled with advanced optimization techniques such as genetic algorithms, they further enhance process efficiency and precision in laser welding [25-26] as well as Resistance Spot Welding [27]. Gaussian Process Regression (GPR) and Fuzzy logic models offer an added advantage by quantifying uncertainty in predictions, which is critical for safety-critical FSW applications [28-29]. For defect prediction and prevention, finite element modelling (FEM) of coupled thermo-mechanical phenomena enables the simulation of temperature fields, material flow, and defect-prone zones, providing physically interpretable insights for process optimization [30]. Non-destructive testing (NDT) techniques such as ultrasonic C-scans and radiography, combined with image processing, have been successfully employed to detect and size internal defects, which are then correlated to reductions in tensile strength and fatigue performance [31-32]. Hybrid approaches that integrate physics-based FEM outputs, statistical surrogates, and NDT features have recently emerged as a promising route to achieve high prediction accuracy with interpretable models, avoiding the black-box nature of ANN-based methods, while supporting real-time quality monitoring in industrial FSW applications.

Based on previous literature, various techniques have been employed to predict the accuracy of mechanical properties for a limited number of datasets, particularly for single materials or alloys. However, a gap exists in integrating data from different aluminium alloys in the context of welding to predict the accuracy of mechanical properties. This paper aims to address that gap by collecting datasets from various aluminium alloys, specifically Al 2024, Al 2219, and Al 6061, to predict the accuracy of yield strength and welding defects. The study utilizes an artificial neural network (ANN) to analyse data from 100 different datasets.

2. DATASET COLLECTION

One hundred sets of data for the FSW of three aluminium alloys [33-35], AA2024, AA2219 and AA6061 obtained from the peer-reviewed literature in table 1. These data sets are used for the present work. The literature reviews for AA2024 reported that variations in tool rotation speed, traverse speed, and probe design significantly influence grain refinement, hardness distribution, and tensile strength, with threaded probes improving material flow and reducing defects [36-38]. In AA2219, the researchers highlighted its high sensitivity to welding conditions,

with efforts focused on analysing microstructural changes, and applying non-destructive testing (NDT) to identify defects such as voids and tunnels; optimized parameters were shown to refine grains and enhance tensile efficiency [40-43].

Similarly, investigations on AA6061 emphasized the influence of process parameters on tensile behaviour, internal defect formation, and surface quality, showing that properly optimized rotational and traverse speeds can achieve joint strengths close to that of the base metal while minimizing tunnel defects and improving surface finish [44-46]. Collectively, these studies highlight that, while all three alloys benefit from refined microstructures and improved mechanical properties under optimized FSW conditions, AA2024 and AA2219 exhibit greater defect sensitivity compared to the relatively more weldable AA6061.

From the previous literature reviews, these data are used for predicting yield strength and welding defects using an artificial neural network.

Table 1. Data set collection detail for three types for Al alloy

Sample	Types of Al alloy	No of data sets
1	2024	20
2	2219	35
3	6061	45

Table 2. Chemical composition for AA2024, AA2219, and AA6061 [47-50]

Material	Si	Cu	Fe	Zn	Mg	Mn	Cr	Al	V	Zr	Ti
AA2024	0.3	4.4	0.3	0.22	2.3	0.04	0.1	Bal	-	-	-
AA2219	0.18	6.5	0.30	0.10	0.03	0.42	-	Bal	0.13	0.23	0.12
AA6061	0.5-0.9	0.14-0.40	0.0-0.08	0.0-0.23	0.7-0.13	0.0-0.13	0.04-0.32	95.80-97.56	-	-	0.02-0.26

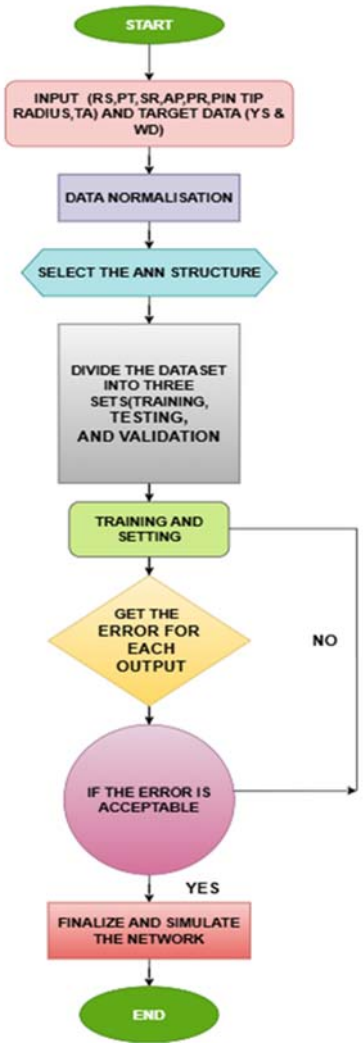

Fig. 1. Flow chart for ANN process

3. ANN PROCESS

The development of the ANN model for predicting yield strength and welding defects follows a systematic procedure, as illustrated in the flow diagram (Fig. 1). Initially, the input process variables such as rotational speed (RS), Plate thickness (PT), Shoulder radius (SR), axial pressure (AP), pin root radius (PR), pin tip radius (PS), and tool angle (TA) are provided along with the target data, namely yield strength (YS) and weld defect (WD). To ensure uniformity and to prevent the dominance of higher-magnitude variables, the dataset is subjected to normalization, typically by scaling the values within a predefined range from 0 to 1. Following normalization, the ANN structure is selected by defining the number of input neurons, hidden layers, hidden neurons, and output neurons. The dataset is then divided into three subsets: training, testing, and validation.

The network is trained iteratively until convergence is achieved. At each training cycle, the prediction error for each output parameter is calculated. If the error level is found to be unacceptable, the training is repeated with modified weights or network settings. Once the error falls within the acceptable range, the final ANN model is obtained. The finalized network is then simulated to predict target output responses.

4. RESULTS AND DISCUSSION

MATLAB R2016a was employed to forecast the output response of the yield strength of the al alloy friction stir-welded (FSW) joints. The experimental results obtained from Kaggle datasets served as the primary

input-output data source for training and testing the ANN model.

The experimental dataset consisting of 100 samples divided into three subsets: 70% for training to establish the model (70 data sets), 15% for testing (15 datasets), and 15% for validation (15 datasets) to assess the generalization ability of the network. This partitioning was carried out using Neural Network Toolbox [51-52]. The iterative evaluation of these network structures ensured the selection of an optimal model capable of capturing the complex nonlinear relationships between welding parameters and mechanical properties of the FSW joint.

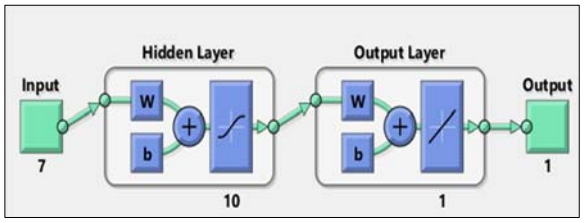

Fig. 2. The ANN structure

The MLP neural network model employed in this study utilizes the Tangential-Sigmoid (tansig) activation function for the hidden layer and a linear transfer function for the output layer, ensuring effective nonlinear mapping of input variables to the output response. For the training phase, LM backpropagation algorithm was implemented, as it is widely regarded for its fast convergence and superior efficiency in handling medium-sized datasets. The developed ANN architecture is defined as a (7–10–1) structure (Fig. 2), representing seven input nodes corresponding to welding process parameters, ten hidden layers with ten neurons optimized through trial-and-error evaluation, and one output node corresponding to the predicted response. To comprehensively evaluate the predictive performance of the ANN model for yield strength of the joints, two key statistical indices were employed which are the coefficient of determination (R) and the mean squared error (MSE) [53]. Their formulae are shown in equations (1) and (2) respectively [54-55]. These metrics provide insight into both the accuracy and robustness of the model across different datasets. The dataset was partitioned into training, validation, and testing subsets. R along with MSE values were calculated separately for each phase to avoid bias in model assessment.

$$R = \frac{\sum(y_i-\bar{y})(x_i-\bar{x})}{\sqrt{\sum(y_i-\bar{y})^2\sum(x_i-\bar{x})^2}} \quad (1)$$

where R is the coefficient of determination, y_i values of the x-variable in a sample, x_i values of the y-variable in a sample.

$$\text{MSE} = \frac{1}{\text{Number of sample}} \sum \text{Square errors} \quad (2)$$

Furthermore, regression analysis was carried out to examine the degree of correlation between the ANN-predicted outputs and the corresponding experimental target values [56].

A regression line with a slope close to unity and an intercept approaching zero indicates strong agreement between predicted and actual results, thereby confirming the ANN's capability to accurately capture the complex nonlinear interactions between input parameters and output responses in the FSW process. The comprehensive regression plots for the ANN model are presented for yield strength in figure 3.

The analysis of correlation coefficients (R) across different dataset partitions revealed excellent agreement between the predicted and experimental values of yield strength. Specifically, the correlation coefficients obtained for the training, validation, and testing values were 0.96568, 0.99874, and 0.96278, respectively. The overall correlation coefficient was found to be 0.96764**,** confirming the robustness of the model.

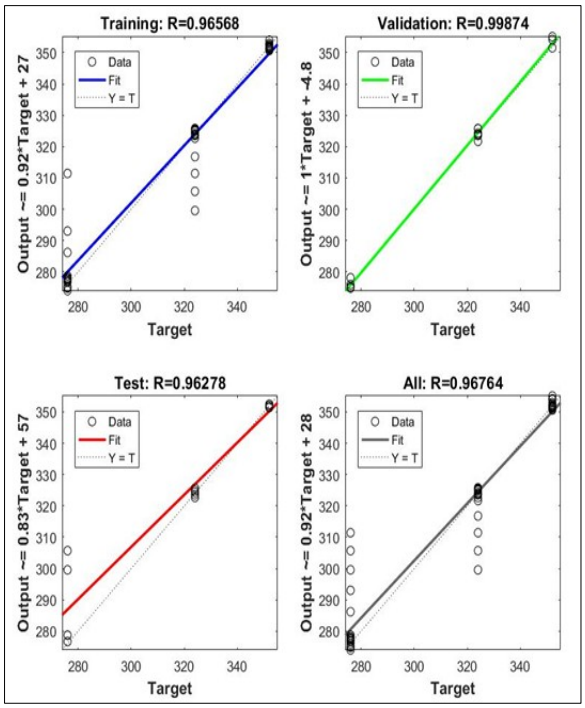

Fig. 3. Regression fit for yield strength

Figure 4 shows the error histogram, which quantifies the deviations between predicted and actual responses. The histogram is divided into bins, each representing a specific error range, with the Y-axis indicating the number of samples within each bin. For both the training and validation datasets, the maximum bin height is approximately 70, revealing that the majority of prediction errors fall within the narrow range of 0.9946, signifying high model precision.

Notably, the zero-error line appears slightly offset to the left of the central bin, but it also corresponds to the same minimal error of 0.9946. The majority of the

samples are concentrated around the zero-error line, with the highest frequency observed between approximately -33.92 and +22.95, indicating that most predictions are highly accurate and closely aligned with the actual values. The blue (training), green (validation), and red (testing) bars are clustered near zero, confirming that the model generalizes well across all datasets without significant overfitting. Only a small number of instances fall into the extreme error ranges which represent outliers but have negligible influence compared to the dominant cluster near zero.

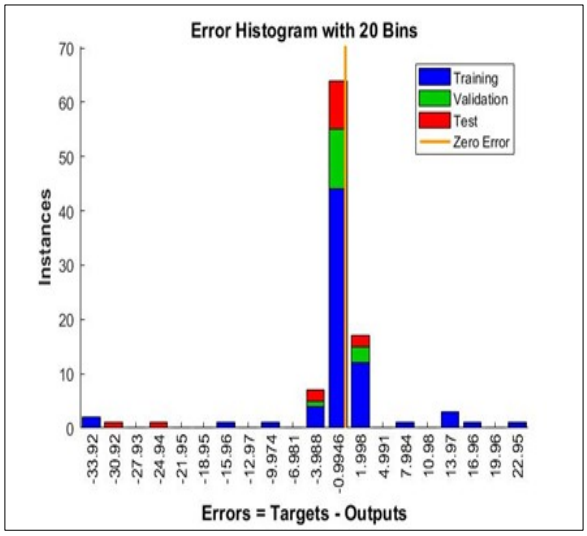

Fig. 4. Error histogram plot for yield strength

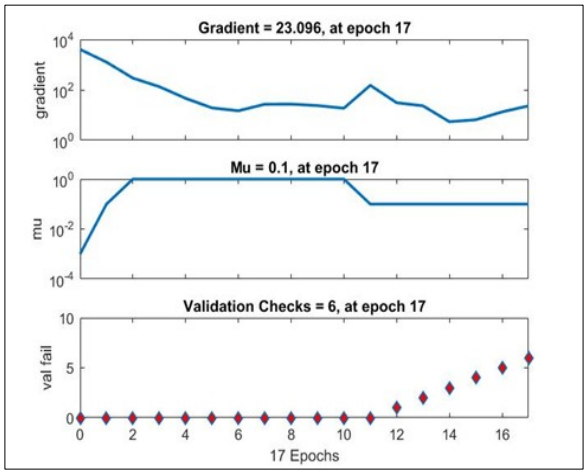

Fig. 5. Training state diagram for yield strength

From figure 5, the training state diagram illustrates the convergence behaviour of the ANN during 17 epochs by tracking gradient, Mu, and validation checks. The gradient, which reflects the rate of change of the error concerning the weights, shows a steady decline from 10^4 to 10^1, reaching 23.096 at epoch 17, indicating that the network moved progressively toward convergence. The validation checks curve reveals that after six consecutive failures to reduce validation error, training was terminated at epoch 17, demonstrating the use of early stopping to avoid overfitting.

From figure 6, the performance plot illustrates the variation of MSE for training, validation, and testing datasets over 17 epochs. The validation error reaches its lowest point at 2.1901 during epoch 11, marking the optimal generalization performance of the ANN, after which it begins to rise slightly, signalling the onset of overfitting. This demonstrates that the ANN model achieves its best predictive capability at epoch 11, with minimal error and strong agreement between predicted and experimental values, while further training offers no improvement and may reduce generalization accuracy.

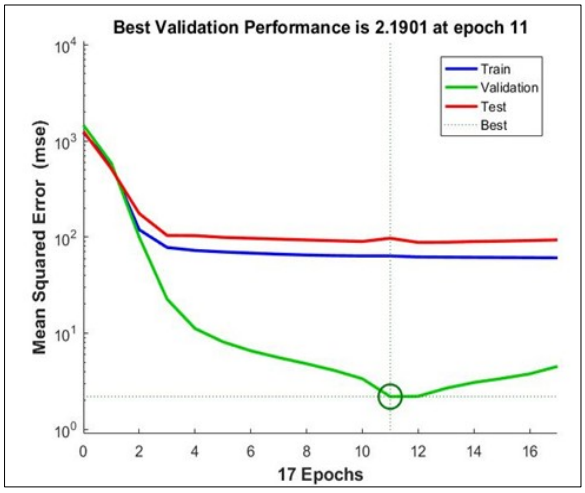

Fig. 6. Best validation curve for yield strength

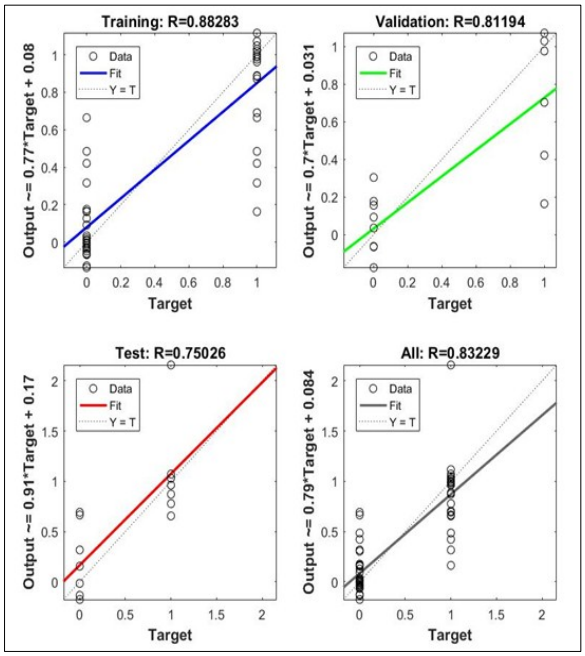

Fig. 7. Regression fit for welding defects

From the ANN model results for yield strength, it demonstrates outstanding predictive accuracy,

achieving a relative discrepancy of less than 1% between predicted and experimental values, thereby validating its ability to accurately capture the complex nonlinear interactions between seven process parameters and output response (yield strength). The comprehensive regression plots for ANN model is presented for welding defect in figure 7. The analysis of correlation coefficients (R) across different dataset partitions revealed excellent agreement between the predicted and experimental values of yield strength. Specifically, the correlation coefficients obtained for the training, validation, and testing values were 0.88283, 0.81194, and 0.75026, respectively. The overall correlation coefficient was found to be 0.83229. The regression plots reveal that the predicted outputs closely align with experimental targets, even though slight deviations in the test dataset suggest the presence of experimental variability.

Figure 8 shows the error histogram for welding defect. The maximum bin height is approximately 35, revealing that the majority of prediction errors fall within the narrow range of 0.01109, denoting high model precision. Notably, the zero-error line appears slightly offset to the right of the central bin and its minimal error of 0.01109. Samples are concentrated around the zero-error line, with the highest frequency observed between approximately –1.108 and +0.7868, indicating that most predictions are highly accurate and closely aligned with the actual values. The highest peak is centred around zero, particularly dominated by training data, which indicates the model has learned the underlying patterns effectively. Small spreads of errors in validation and testing sets (green and red) show that the model generalizes well to unseen data, though slight deviations occur, likely due to experimental variability or noise.

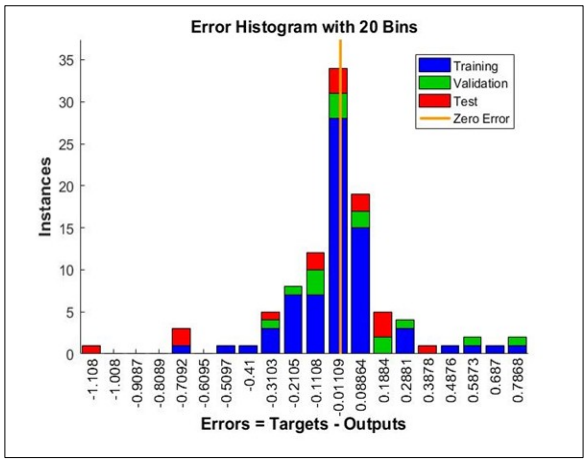

Fig. 8. Error histogram plot for welding defects

From figure 9, the training state diagram illustrates the ANN model for the welding defect during 23 epochs by tracking gradient, Mu, and validation checks. The gradient which reaching 0.014297 at epoch 23, indicating that the network moved progressively toward convergence. The validation checks curve reveals that after six consecutive failures to reduce validation error, training was terminated at epoch 23. The validation error reaches its lowest point at 0.09041 during epoch 17, marking the optimal generalization performance of the ANN, after which it begins to rise slightly, signalling the onset of overfitting (Fig. 10). It is observed that during the early epochs, the errors decrease rapidly across all datasets, showing that the model is quickly learning the underlying patterns. This demonstrates that the ANN model achieves its best predictive capability at epoch 17, with strong agreement between predicted and experimental values.

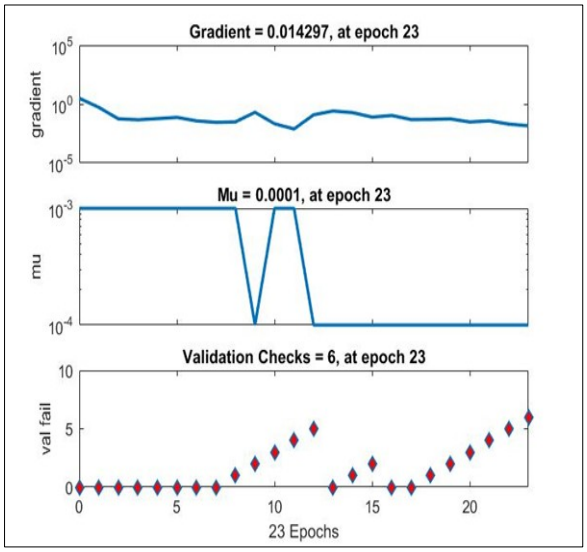

Fig. 9. Training state diagram for welding defects

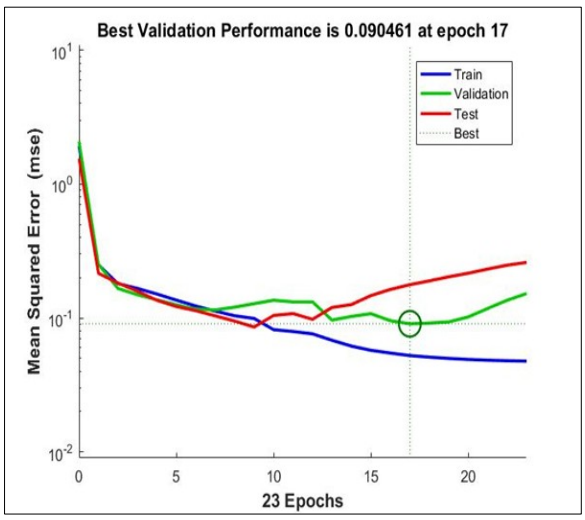

Fig. 10. Best validation curve for welding defects

5. CONCLUSIONS

The findings of this study show that the ANN effectively captures the nonlinear relationships

governing welding defect prediction, providing high predictive accuracy, strong generalization, and reliability for practical applications in welding quality assessment. Several significant conclusions:

- The results demonstrate the effectiveness of the ANN model in predicting the yield strength (YS) and welding defects (WD) of friction stir welded joints made from three aerospace-grade aluminium alloys, namely AA2024, AA2219, and AA6061. A dataset of one hundred experimental cases extracted from peer-reviewed literature was used, incorporating key process parameters rotational speed (RS), plate thickness (PT), shoulder radius (SR), axial pressure (AP), pin root radius (PR), pin tip radius (PS), and tool angle (TA) as inputs, with YS and WD as outputs. The ANN, configured in a (7–10–1) architecture and implemented in MATLAB R2016a, exhibited strong predictive performance.
- For yield strength, the model achieved correlation coefficients of 0.96568, 0.99874, and 0.96278 for training, validation, and testing, respectively, with an overall R of 0.96764. The error histogram confirmed that most prediction errors were confined within a narrow range (0.9946), indicating high accuracy. The minimum validation error (MSE = 2.1901) occurred at epoch 11. For welding defects, correlation coefficients of 0.88283, 0.81194, and 0.75026 were obtained, with an overall R of 0.83229. The error histogram revealed minimal deviation, with the majority of errors concentrated within 0.01109, and the lowest validation error (MSE = 0.09041) recorded at epoch 17 out of 23.
- These results establish the ANN framework as a reliable tool for predicting both yield strength and defect formation in FSW of AA2024, AA2219, and AA6061 alloys. Future work may expand on this approach by integrating larger datasets, exploring hybrid modelling strategies, and extending the methodology to other alloy systems and joining techniques for enhanced predictive capabilities.

REFERENCES

[1] **Kaliappan S., Mothilal T., Natrayan L., Pravin P., Olkeba T. T.,** *Mechanical Characterization of Friction-Stir-Welded Aluminum AA7010 Alloy with TiC Nanofiber,* Advances in Materials Science and Engineering, 2023, vol. 2023, pp. 1-7.

[2] **Manickam S., Pradeep A., Vijayakumar S., Mosisa E.,** *Optimization of arc welding process parameters for joining dissimilar metals,* Materials Today Proceedings, 2022, vol. 69, pp. 662-664.

[3] **Anand R., Padmanabhan R.,** *Influence of friction stir welding process parameters and statistical behaviour of the novel interlock aluminum alloys joint with SiCp reinforcement,* CIRP Journal of Manufacturing Science and Technology, 2023, vol. 45, pp. 260-270.

[4] **Praveen R., Koteswara Rao S. R., Selvakumar G., Damodaram R.,** *High-Velocity Projectile Impact Behaviour of Friction Stir Welded AA7075 Thick Plates,* Defence Technology, 2023, vol. 29, pp. 153-163.

[5] **Venkatesh R. et al.,** *Influence of Different Frequency Pulse on Weld Bead Phase Ratio in Gas Tungsten Arc Welding by Ferritic Stainless Steel AISI-409L,* Journal of Nanomaterials, 2022, vol. 2022, iss. 1, 9530499.

[6] **Abdeltawab N. M., Elshazly M., Shash A. Y., El-Sherbiny M.,** *Study the effect of processing parameters on friction stir welding of AA5083 aluminum alloy reinforced with Al-SiC matrix,* Results in Materials, 2025, vol. 27, p. 100731.

[7] **Yuk S. et al.,** *Micro/nanostructure evolution and deformation mechanisms in friction-stir-welded 7075 Al alloy: A comparative analysis of weld zones,* Journal of Materials Research and Technology, 2025, vol. 36, pp. 5193-5210.

[8] **Mishra R. S., Ma Z. Y.,** *Friction stir welding and processing,* Materials Science and Engineering R Reports, 2005, vol. 50, iss. 1-2, pp. 1-78.

[9] **Kaliappan S., Balaji V., Mohan Raj N., Yatika G., Natrayan L., Shyam D.,** *Friction stir welding of nylon 6-6 thick plates using biochar colloidal nanoparticle,* Materials Today Proceedings, 2023, https://doi.org/10.1016/j.matpr.2023.03.007.

[10] **Yan J., Sutton M. A., Reynolds A. P.,** *Process-structure-property relationships for nugget and heat affected zone regions of AA2524-T351 friction stir welds,* Science and Technology of Welding and Joining, 2005, vol. 10, iss. 6, pp. 725-736.

[11] **Li Y., Sun D., Gong W.,** *Effect of Tool Rotational Speed on the Microstructure and Mechanical Properties of Bobbin Tool Friction Stir Welded 6082-T6 Aluminum Alloy*, Metals (Basel), vol. 9, iss. 8, p. 894.

[12] **Ilangovan M., Rajendra Boopathy S., Balasubramanian V.,** *Effect of tool pin profile on microstructure and tensile properties of friction stir welded dissimilar AA 6061-AA 5086 aluminium alloy joints*, Defence Technology, vol. 11, iss. 2, pp. 174-184.

[13] **Chen Y., Li Y., Shi L., Wu C., Li S., Gao S.,** *Optimizing the shoulder diameter for double side friction stir welding of medium-thick TC4/AA2024 dissimilar alloys by Taguchi optimization technique*, Welding in the World, vol. 67, iss. 8, pp. 1887-1899.

[14] **Jata K. V., Semiatin S. L.,** *Continuous dynamic recrystallization during friction stir welding of high strength aluminum alloys*, Scripta Materialia, vol. 43, iss. 8, pp. 743-749.

[15] **Padhy G. K., Wu C. S., Gao S.,** *Friction stir based welding and processing technologies - processes, parameters, microstructures and applications: A review*, Journal of Materials Science and Technology, vol. 34, iss. 1, pp. 1-38.

[16] **Kumar K., Kailas S. V.,** *The role of Friction Stir Welding Tool on Material Flow and Weld Formation*, Materials Science and Engineering A, vol. 485, iss. 1-2, pp. 367-374.

[17] **Sato Y. S., Urata M., Kokawa H.,** *Parameters controlling microstructure and hardness during friction-stir welding of precipitation-hardenable aluminum alloy 6063*, Metallurgical and Materials Transactions A, vol. 33, iss. 3, pp. 625-635.

[18] **Kundu J., Singh H.,** *Friction Stir Welding of AA5083 Aluminium Alloy: Multi-response optimization using Taguchi-based grey relational analysis*, Advances in Mechanical Engineering, vol. 8, iss. 11.

[19] **Rai R., De A., Bhadeshia H. K. D. H., DebRoy T.,** *Review: Friction stir welding tools*, Science and Technology of Welding and Joining, vol. 16, iss. 4, pp. 325-342.

[20] **Matitopanum S., Pitakaso R., Sethanan K., Srichok T., Chokanat P.,** *Prediction of the Ultimate Tensile Strength (UTS) of Asymmetric Friction Stir Welding Using Ensemble Machine Learning Methods*, Processes, vol. 11, iss. 2, p. 391.

[21] **Ghetiya N. D., Patel K. M.,** *Prediction of Tensile Strength in Friction Stir Welded Aluminium Alloy Using Artificial Neural Network*, Procedia Technology, vol. 14, pp. 274-281.

[22] **Dewan M. W., Huggett D. J., Liao T. Warren, Wahab M. A., Okeil A. M.,** *Prediction of tensile strength of friction stir weld joints with adaptive neuro-fuzzy inference system (ANFIS) and neural network*, Materials & Design, vol. 92, pp. 288-299.

[23] **Cho M., Gim J., Kim J. H., Kang S.,** *Development of an Artificial Neural Network Model to Predict the Tensile Strength of Friction Stir Welding of Dissimilar Materials Using Cryogenic Processes*, Applied Sciences, vol. 14, iss. 20, p. 9309.

[24] **Li X., Simpson S. W., Rados M.,** *Neural networks for online prediction of quality in gas metal arc welding*, Science and Technology of Welding and Joining, vol. 5, iss. 2, pp. 71-79.

[25] **Acherjee B., Mondal S., Tudu B., Misra D.,** *Application of artificial neural network for predicting weld quality in laser transmission welding of thermoplastics*, Applied Soft Computing, vol. 11, iss. 2, pp. 2548-2555.

[26] **Yuguang Z.**, **Kai X.**, **Dongyan S.**, *An improved artificial neural network for laser welding parameter selection and prediction*, International Journal of Advanced Manufacturing Technology, vol. 68, iss. 1-4, pp. 755-762.
[27] **Lin H.-L.**, **Chou T.**, **Chou C.-P.**, *Optimization of resistance spot welding process using Taguchi method and a neural network*, Experimental Techniques, vol. 31, iss. 5, pp. 30-36.
[28] **Hartl R.**, **Vieltorf F.**, **Benker M.**, **Zaeh M. F.**, *Predicting the Ultimate Tensile Strength of Friction Stir Welds Using Gaussian Process Regression*, Journal of Manufacturing and Materials Processing, vol. 4, iss. 3, p. 75.
[29] **Mystica A.**, **Senthil Kumar V. S.**, **Sakthi Abirami B.**, *Analysis and prediction of uncertain responses using regression and fuzzy logic for friction stir welding of AA2014 under n-MQL*, Journal of Intelligent & Fuzzy Systems, vol. 43, iss. 3, pp. 2375-2390.
[30] **Zhu Z.**, **Wang M.**, **Zhang H.**, **Zhang X.**, **Yu T.**, **Wu Z.**, *A Finite Element Model to Simulate Defect Formation during Friction Stir Welding*, Metals (Basel), vol. 7, iss. 7, p. 256.
[31] **Tabatabaeipour M.**, **Hettler J.**, **Delrue S.**, **Van Den Abeele K.**, *Non-destructive ultrasonic examination of root defects in friction stir welded butt-joints*, NDT & E International, vol. 80, pp. 23-34.
[32] **Sudhagar S.**, **Sakthivel M.**, **Ajith Arul Daniel S.**, *Application of image processing to radiographic image for quantitative assessment of friction stir welding quality of aluminium 2024 alloy*, Measurement, vol. 152, p. 107294.
[33] **Baruah A.**, **Borkar H.**, *Optimised machine learning classification model to detect void formations in friction stir welding*, Materials Today: Proceedings, Mar. 2023.
[34] **Zhao C.**, **Pei X.**, **Liu X.**, *Computational investigation on void defects formation and periodic tool-workpiece sliding-to-sticking transition in self-reacting friction stir welding*, International Journal of Advanced Manufacturing Technology, vol. 120, iss. 11-12, pp. 8075-8088.
[35] **Baruah A.**, *Void formation process data in welding [Dataset]*, Kaggle, 2023, https://www.kaggle.com/datasets/arindambaruah/void-formation-process-data-in-welding.
[36] **Anil Kumar H. M.**, **Venakata Ramana V.**, **Shanmuganathan S. P.**, *Experimental Investigation of Mechanical Properties And Morphological Studies on Friction Stir Welded Aluminum 2024 Alloy*, Materials Today: Proceedings, vol. 5, iss. 1, pp. 700-708.
[37] **Carlone P.**, **Palazzo G. S.**, *Influence of Process Parameters on Microstructure and Mechanical Properties in AA2024-T3 Friction Stir Welding*, Metallography, Microstructure, and Analysis, vol. 2, iss. 4, pp. 213-222.
[38] **Mahmudi E.**, **Farhangi H.**, *The Influence of Welding Parameters on Tensile Behavior of Friction Stir Welded Al 2024-T4 Joints*, Advanced Materials Research, vol. 83-86, pp. 1197-1204.
[39] **Nejad S. G.**, **Yektapour M.**, **Akbarifard A.**, *Friction stir welding of 2024 aluminum alloy: Study of major parameters and threading feature on probe*, Journal of Mechanical Science and Technology, vol. 31, iss. 11, pp. 5435-5445.
[40] **Li B.**, **Shen Y.**, **Hu W.**, *The study on defects in aluminum 2219-T6 thick butt friction stir welds with the application of multiple non-destructive testing methods*, Materials & Design, vol. 32, iss. 4, pp. 2073-2084.
[41] **Lee H.-S.**, **Yoon J.-H.**, **Yoo J.-T.**, **Min K.-J.**, *A Study on Microstructure of AA2219 Friction Stir Welded Joint*, in Proceedings of the International Symposium on Mechanical Engineering and Material Science, Paris, France: Atlantis Press, 2016.
[42] **Lakshminarayanan A. K.**, **Malarvizhi S.**, **Balasubramanian V.**, *Developing friction stir welding window for AA2219 aluminium alloy*, Transactions of Nonferrous Metals Society of China, vol. 21, iss. 11, pp. 2339-2347.
[43] **Liu H.**, **Zhang H.**, **Pan Q.**, **Yu L.**, *Effect of friction stir welding parameters on microstructural characteristics and mechanical properties of 2219-T6 aluminum alloy joints*, International Journal of Material Forming, vol. 5, iss. 3, pp. 235-241.
[44] **Lim S.**, **Kim S.**, **Lee C.-G.**, **Kim S.**, *Tensile behavior of friction-stir-welded Al 6061-T651*, Metallurgical and Materials Transactions A, vol. 35, iss. 9, pp. 2829-2835.
[45] **Ramulu P. J.**, **Narayanan R. G.**, **Kailas S. V.**, **Reddy J.**, *Internal defect and process parameter analysis during friction stir welding of Al 6061 sheets*, International Journal of Advanced Manufacturing Technology, vol. 65, iss. 9-12, pp. 1515-1528.
[46] **Feng T. T.**, **Zhang X. H.**, **Fan G. J.**, **Xu L. F.**, *Effect of the rotational speed on the surface quality of 6061 Al-alloy welded joint using friction stir welding*, IOP Conference Series: Materials Science and Engineering, vol. 213, p. 012047.
[47] **Yadav A.**, **Mehmood A.**, *Optimization of Process parameters of friction stir welded joint of dissimilar Al-alloy AA2024 and AA5052 using response surface methodology*, International Journal of Research in Engineering and Innovation, vol. 4, iss. 1, pp. 69-76.
[48] **Kaufman J. G.**, **Nelson F. G.**, **Johnson E. W.**, *The Properties of Aluminum Alloy 2219 Sheet, Plate, and Welded Joints at Low Temperatures*, in Advances in Cryogenic Engineering, Boston, MA: Springer US, 1963, pp. 661-670.
[49] **Liu H. J.**, **Li J. Q.**, **Duan W. J.**, *Friction stir welding characteristics of 2219-T6 aluminum alloy assisted by external non-rotational shoulder*, International Journal of Advanced Manufacturing Technology, vol. 64, iss. 9-12, pp. 1685-1694.
[50] **Kareem A.**, **Qudeiri J. A.**, **Abdudeen A.**, **Ahammed T.**, **Ziout A.**, *A Review on AA 6061 Metal Matrix Composites Produced by Stir Casting*, Materials (Basel), vol. 14, iss. 1, p. 175.
[51] **Aruri D.**, **Adepu K.**, **Adepu K.**, **Bazavada K.**, *Wear and mechanical properties of 6061-T6 aluminum alloy surface hybrid composites [(SiC+Gr) and (SiC+Al2O3)] fabricated by friction stir processing*, Journal of Materials Research and Technology, vol. 2, iss. 4, pp. 362-369.
[52] **Jeyakrishnan S.**, **Vijayakumar S.**, **Naga Swapna Sri M.**, **Anusha P.**, *An integration of RSM and ANN modelling approach for prediction of FSW joint properties in AA7178/AA5456 alloys*, Canadian Metallurgical Quarterly, vol. 64, iss. 1, pp. 43-60.
[53] **Abdollah-Zadeh A.**, **Saeid T.**, **Sazgari B.**, *Microstructural and mechanical properties of friction stir welded aluminum/copper lap joints*, Journal of Alloys and Compounds, vol. 460, iss. 1-2, pp. 535-538.
[54] **Ocampo I.**, **López R. R.**, **Camacho-León S.**, **Nerguizian V.**, **Stiharu I.**, *Comparative Evaluation of Artificial Neural Networks and Data Analysis in Predicting Liposome Size in a Periodic Disturbance Micromixer*, Micromachines, vol. 12, iss. 10, p. 1164.
[55] **Imbens G. W.**, **Newey W. K.**, **Ridder G.**, *Mean-square-error Calculations for Average Treatment Effects*, SSRN Electronic Journal, 2005.
[56] **Ma X.**, *Effect of Temperature and Material Flow Gradients on Mechanical Performances of Friction Stir Welded AA6082-T6 Joints*, Materials (Basel), vol. 15, iss. 19, p. 6579.